Large-Scale Patterns in a Minimal Cognitive Flocking Model: Incidental Leaders, Nematic Patterns, and Aggregates

Lucas Barberis[1,2] and Fernando Peruani[1,*]
[1]Université Côte d'Azur, Laboratoire J.A. Dieudonné, UMR 7351 CNRS, Parc Valrose, F-06108 Nice Cedex 02, France
[2]IFEG, FaMAF, CONICET, UNC, X5000HUA Córdoba, Argentina

(Received 11 June 2016; revised manuscript received 26 August 2016; published 6 December 2016)

We study a minimal cognitive flocking model, which assumes that the moving entities navigate using the available instantaneous visual information exclusively. The model consists of active particles, with no memory, that interact by a short-ranged, position-based, attractive force, which acts inside a vision cone (VC), and lack velocity-velocity alignment. We show that this active system can exhibit—due to the VC that breaks Newton's third law—various complex, large-scale, self-organized patterns. Depending on parameter values, we observe the emergence of aggregates or millinglike patterns, the formation of moving—locally polar—files with particles at the front of these structures acting as effective leaders, and the self-organization of particles into macroscopic nematic structures leading to long-ranged nematic order. Combining simulations and nonlinear field equations, we show that position-based active models, as the one analyzed here, represent a new class of active systems fundamentally different from other active systems, including velocity-alignment-based flocking systems. The reported results are of prime importance in the study, interpretation, and modeling of collective motion patterns in living and nonliving active systems.

DOI: 10.1103/PhysRevLett.117.248001

It is believed that complex, self-organized, collective motion patterns observed in birds, fish, or sheep [1–6] as well as nonliving active systems [7–10] result from the presence of a velocity alignment mechanism that mediates the interactions among the moving individuals. Such a velocity alignment mechanism is at the core of the so-called Vicsek-like models [11] extensively used to study flocking patterns [1,2]. Intrinsically nonequilibrium, these patterns differ remarkably from those observed in equilibrium systems by the lack of both Galilean invariance and momentum conservation, which allows, for instance, the emergence of long-range orientational order in two dimensions [11–13] and the presence of anomalous density fluctuations [14,15].

Few recent pioneering works [16–23] have challenged the wide-spread view that behind each collective motion pattern of self-propelled entities, there is a velocity alignment mechanism at work. Here, we explore the possibility of observing flocking patterns in the absence of such alignment. The model we analyze is a minimal cognitive flocking model that assumes that the moving entities navigate using exclusively the instantaneous visual information they receive. Importantly, the moving particles have no memory so as to compute the moving direction of neighboring particles, in sharp contrast to standard flocking models [1,2,11]. The navigation strategy we investigate is based on the instantaneous position of neighboring particles and not on their velocity, which makes the model simpler from a cognitive point of view and computationally less intensive, providing an alternative in the design of robotic navigation algorithms. The model incorporates few well-known physiological and cognitive concepts. For instance, we assume that particles are attracted by those particles located inside the vision cone. The vision cone (VC) results from two well-documented facts: (i) animals have a limited field of view [18,24,25]—typically less than 360°—which is parametrized here by the angle β, and (ii) when navigating, objects located at far distances are ignored, and the focus is put on those objects located at distances shorter than the so-called cognitive horizon

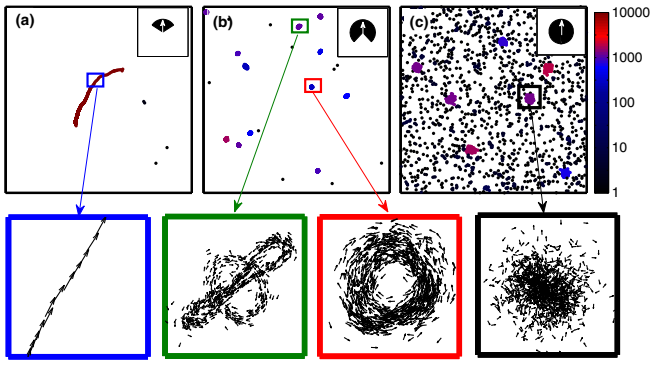

FIG. 1. Depending on vision cone size β (insets), we can observe the formation of locally polar structures, which we call "worms," panel (a)—$\beta = 0.8$, or the emergence of aggregates or millinglike patterns as shown in panel (b) for $\beta = 2.4$, and panel (c) for $\beta \sim \pi$. Parameters (a)–(c): $\sqrt{2D_\theta} = 0.12$, $L = 100$, $N = 10^4$. See [45] for movies.

[18,24,26] that corresponds in our model to R_0. The field of view (β) is known to vary from species to species, being, for instance, smaller for predators than for preys [24,25]. In summary, the field of view (β) combined with the cognitive horizon (R_0) defines the VC, which violates Newton's third law for $\beta < \pi$. Notice that alternative mechanisms exist to break the action-reaction symmetry to the VC [23,27,28], and that the presence of nonreciprocal interactions also has a strong impact on the dynamics of flocking models with velocity alignment [29–32].

Here, we show that this minimal cognitive flocking model exhibits various large-scale self-organized patterns, depending on the size of the VC and noise intensity: aggregates or millinglike patterns of various degrees of complexity, locally polar dynamical structures which we call worms (Fig. 1), and nematic bands leading to long-ranged nematic order. Furthermore, we derive a system of nonlinear field equations to rationalize agent-based simulation results and show that, in general position-based active models, as the one studied here, represent a new class of active systems fundamentally different from other active systems, including velocity-alignment-based flocking systems [11–14,33–44].

Model definition.—The equation of motion of the ith particle is given by

$$\dot{\mathbf{x}}_i = v_0 \mathbf{V}(\theta_i);$$
$$\dot{\theta}_i = \frac{\gamma}{n_i} \sum_{j \in \Omega_i} \sin(\alpha_{ij} - \theta_i) + \sqrt{2D_\theta}\xi_i(t), \qquad (1)$$

where $\mathbf{x}_i$ denotes the position of the particle, θ_i represents its moving direction, with $\mathbf{V}(\cdot) \equiv (\cos(\cdot), \sin(\cdot))^T$, v_0 is the particle speed, γ the strength of the interactions, and $\xi_i(t)$ is a noise term such that $\langle \xi_i(t) \rangle = 0$ and $\langle \xi_i(t)\xi_j(t') \rangle = \delta_{i,j}\delta(t - t')$, with the noise amplitude given by D_θ. The sum in Eq. (1) describes the projection on the "retina" of particle i of the position of all particles inside its VC, assuming particles are pointlike, with α_{ij} the polar angle of the vector $(\mathbf{x}_j - \mathbf{x}_i/\|\mathbf{x}_j - \mathbf{x}_i\|) = \mathbf{V}(\alpha_{ij})$; a procedure similar to the one in [19] for long-range interactions. The symbol Ω_i, thus, denotes the set of neighbors inside the VC of particle i, with n_i its cardinal number. Particles in Ω_i are those that satisfy $\|\mathbf{x}_j - \mathbf{x}_i\| \leq R_0$ and $(\mathbf{x}_j - \mathbf{x}_i/\|\mathbf{x}_j - \mathbf{x}_i\|) \cdot (\dot{\mathbf{x}}_i/\|\dot{\mathbf{x}}_i\|) > \cos(\beta)$, with β the size of the cone and its orientation given by $\dot{\mathbf{x}}_i$. For a definition of the model in 3D and a justification of the term $\sin(\alpha_{ij} - \theta_i)$, see [45]. In the following, we fix $v_0 = 1$, set $R_0 = 1$, $\gamma = 5$, and the global density $\rho_0 = N/L^2 = 1$, with N the number of particles and L the linear size of the system and use periodic boundary conditions. These parameters are in the range of the ones expected for vertebrates [48].

Phenomenology.—The system exhibits four distinct phases—see Fig. 2—which we refer to as (i) gas phase, (ii) aggregate phase, (iii) worm phase, and (iv) nematic

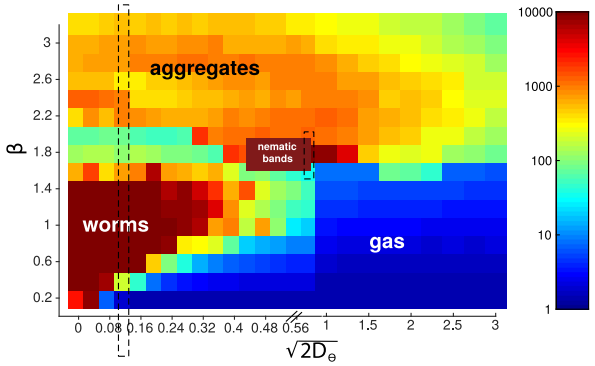

FIG. 2. Phase diagram: vision angle β vs angular noise intensity D_θ. The color code indicates the value of the average cluster size m^* in simulations with $N = 10^4$. Vertical rectangles refer to cuts of the phase diagram shown in Figs. 3 and 4.

phase. Phases (ii) to (iv) involve spontaneous phase separation of the particles, while phase (i) is characterized by the absence of order and a homogeneous distribution of particles in space. In the following, we study the phase-separated phases, i.e., from (ii) to (iv), by performing two vertical cuts in the phase diagram in Fig. 2. The emerging macroscopic patterns are characterized by their level of (global) orientational order through $S_q = |\sum_{j=1}^{N} \exp(iq\theta_j)/N|$, with $q = 1$ for polar order and $q = 2$ for nematic order (and i the imaginary unit). Clustering properties are analyzed by the normalized number of clusters $M^* = \langle M \rangle / N$ and normalize cluster size $m^* = \langle m \rangle / N$, defining a cluster as a set of connected particles, where i is connected to j if j is located inside the VC of i. Finally, transport properties are studied by looking at the behavior of the diffusion coefficient $D_{\text{eff}} = \lim_{t \to \infty} \sum_{i=1}^{N} [\mathbf{x}_i(t) - \mathbf{x}_i(t_0)]^2/[4N(t - t_0)]$.

Aggregate phase.—At large values of β, particles self-organize into aggregates of different complexity, Fig. 1, with some of these patterns comparable to the ones reported in [49]. The aggregates result from a phase separation process (see [45] for movies) fundamentally different from the one in [50,51]. Figure 3(a) shows the existence of different nontrivial scalings of M^* and m^* with time—as expected for active systems [52]—which suggests that the phase-separation process is of a different nature at large and intermediate values of β.

Worm phase.—At lower values of β, we observe the emergence of a new type of macroscopic structure, which we call a worm, Fig. 1(a). This structure consists of a file of active particles that are locally polarly oriented. The particle at the "head" of the worm—which we label "H"—ignores all other particles and becomes the effective leader of the spontaneously formed herd of active particles. This is evident from the behavior of D_{eff} as shown in Fig. 3. During the worm phase, $D_{\text{eff}} \sim D_{\text{NAP}} = v_0^2/(2D_\theta)$, with D_{NAP} the diffusion coefficient of an ensemble of non-interacting active particles (NAP). This is not due to the

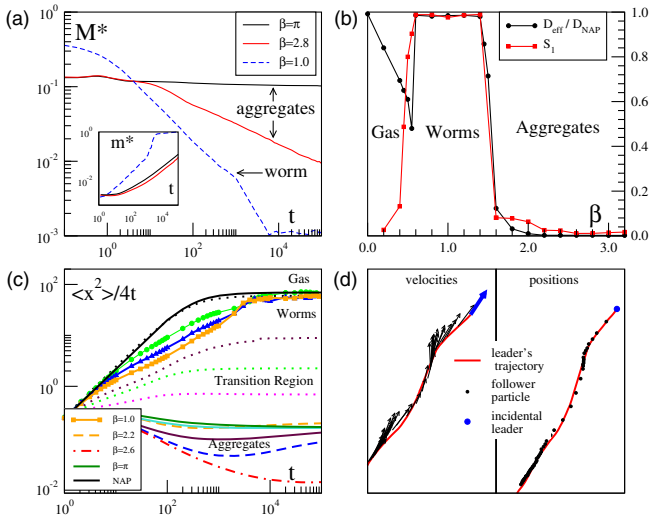

FIG. 3. (a) Normalized number of clusters M^* (normalized average cluster size m^*, inset) as function of time. Worms coagulate at a much faster rate than aggregates. (b) The (normalized) diffusion coefficient $D_{\rm eff}/D_{\rm NAP}$ and polar order S_1 as a function of β (see text). (c) Temporal evolution of $\langle \mathbf{x}^2\rangle/(4t)$. (d) Velocities and positions of particles that form a worm: particles copy the behavior of the particle at the front, which we refer to as the incidental leader. See [45] for a movie. Parameters: $N = 10^4$, $L = 100$, $\sqrt{2D_\theta} = 0.12$.

absence of interaction, but to the fact that all particles in the worm imitate the behavior of the incidental leader particle: the position and velocity of particle j is approximately given by $\mathbf{x}_j(t) \sim \mathbf{x}_H(t - \ell_{j,H}/v_0)$ and $\mathbf{V}(\theta_j(t)) \sim \mathbf{V}(\theta_H(t - \ell_{j,H}/v_0))$, where $\ell_{j,H}$ is the distance along the worm between j and H, see Fig. 3(d) and [45] for a movie. Though worms exhibit local polar order, global polar order drops for $L \gg v_0/D_\theta$, vanishing in the thermodynamic limit.

Nematic phase.—For larger values of D_θ and β, see Figs. 2 and 4, we find macroscopic nematic bands. After a complex transient where various small nematic bands grow in size and interconnect, the system reaches a steady state, with one or several bands, but where only one direction prevails, see Fig. 4 and [45] for a movie. The described dynamics leads to the emergence of genuine global nematic order. Increasing the system size N, for a fixed density ρ_0, we observe that the nematic order S_2 saturates, Fig. 4(a), inset.

Field equations.—A qualitative understanding of the large-scale behavior of the system can be obtained in terms of $p(\mathbf{x},\theta,t) = \langle \sum_{i=1}^N \delta(\mathbf{x}-\mathbf{x}_i)\delta(\theta-\theta_i)\rangle$. The evolution of $p(\mathbf{x},\theta,t)$ is given by the corresponding nonlinear Fokker-Planck equation of Eq. (1) [47]

$$\partial_t p + \boldsymbol{\nabla}[v_0 \mathbf{V}(\theta) p] = D_\theta \partial_{\theta\theta} p - \partial_\theta[\mathcal{I} p], \tag{2}$$

where we have assumed that $p_2(\mathbf{x},\theta,\mathbf{x}',\theta',t) \simeq p(\mathbf{x},\theta,t)p(\mathbf{x}',\theta',t)$ in order to define, after some simple calculations [45], an average interaction term

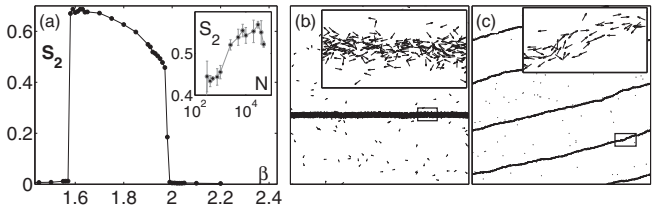

FIG. 4. Nematic bands. (a) The nematic order parameter S_2 as a function of β for $\sqrt{2D_\theta} = 0.84$. The inset shows S_2 as a function of N, with error bars obtained using 50 realizations, $\beta = 1.9$. (b) and (c) display simulation snapshots at the steady state for $N = 10^4$, $L = 100$, $\sqrt{2D_\theta} = 0.84$, and $\beta = 1.9$. Insets in (b) and (c) correspond to magnified views of the bands. See [45] for movies.

$$\mathcal{I} = \Gamma \int_0^{R_0} dR \int_{\theta-\beta}^{\theta+\beta} d\alpha R \sin(\alpha-\theta)\rho[\mathbf{x} + R\mathbf{V}(\alpha), t], \tag{3}$$

where $\Gamma \simeq \gamma/(1+\beta R_0^2 \rho)$ and $\rho[\mathbf{x},t] = \mathcal{L}[1]$ the coarse-grained one-particle density, with $\mathcal{L}[(\cdot)]$ an averaging operator defined as $\mathcal{L}[(\cdot)] \equiv \int_0^{2\pi} d\theta (\cdot) p(\mathbf{x},\theta,t)$. To analyze the behavior of Eq. (2), in addition to $\rho(\mathbf{x},t)$, we introduce the following fields: local polar order $\mathbf{P} \equiv (P_x, P_y)^T = \mathcal{L}[\mathbf{V}(\theta)]$, local nematic order $\mathbf{Q} \equiv (Q_c, Q_s)^T = \mathcal{L}[\mathbf{V}(2\theta)]$, and higher order fields are denoted by $\mathbf{M}_k \equiv (M_{kc}, M_{ks})^T = \mathcal{L}[\mathbf{V}(k\theta)]$ where $k > 2$ corresponds to the local kth order field, and recast the equation as

$$\partial_t \rho + v_0 \nabla \mathbf{P} = 0, \tag{4a}$$

$$\partial_t \mathbf{P} + \frac{v_0}{2}(\nabla\rho + [\nabla^T \overline{\overline{\mathcal{M}}}_Q]^T) = -D_\theta \mathbf{P} - \frac{\Gamma g(\beta)}{2}[\overline{\overline{\mathcal{M}}}_Q - \rho \mathbb{1}]\nabla\rho - \frac{\Gamma f(\beta)}{2}\overline{\overline{\mathcal{M}}}_{\rho 1}[\mathbf{P} - \mathbf{M}_3], \tag{4b}$$

$$\partial_t \mathbf{Q} + \frac{v_0}{2}[\nabla^T(\overline{\overline{\mathcal{M}}}_3 + \overline{\overline{\mathcal{M}}}_P)]^T = -4D_\theta \mathbf{Q} - \Gamma g(\beta)[\overline{\overline{\mathcal{M}}}_3 - \overline{\overline{\mathcal{M}}}_P^T]\nabla\rho - \Gamma f(\beta)\left(\overline{\overline{\mathcal{M}}}_{\rho 2}\mathbf{M}_4 + \rho\begin{bmatrix}\Phi\rho \\ -\partial_{xy}\rho\end{bmatrix}\right), \tag{4c}$$

where the symbols $\overline{\overline{\mathcal{M}}}_A$ denote matrices defined using the auxiliary matrices $\mathbb{E}_1 = \left[\begin{smallmatrix}1 & 0\\ 0 & -1\end{smallmatrix}\right]$, $\mathbb{E}_2 = \left[\begin{smallmatrix}0 & 1\\ 1 & 0\end{smallmatrix}\right]$, $E_3 = \left[\begin{smallmatrix}0 & 1\\ -1 & 0\end{smallmatrix}\right]$, and the unity matrix $\mathbb{1}$ as: $\overline{\overline{\mathcal{M}}}_Q = Q_c\mathbb{E}_1 + Q_s\mathbb{E}_2$, $\overline{\overline{\mathcal{M}}}_3 = M_{3c}\mathbb{E}_1 + M_{3s}\mathbb{E}_2$, $\overline{\overline{\mathcal{M}}}_P = P_x\mathbb{E}_2 + P_y\mathbb{E}_3$, $\overline{\overline{\mathcal{M}}}_{\rho 1} = \Phi\rho/2\mathbb{E}_1 - \partial_{xy}\rho\mathbb{1}$, and $\overline{\overline{\mathcal{M}}}_{\rho 2} = \partial_{xy}\rho\mathbb{E}_2 - \Phi\rho/2\mathbb{E}_1$. In addition, we have defined $\Phi\rho$ as $\Phi\rho = \partial_{yy}\rho - \partial_{xx}\rho$ and the terms $g(\beta)$ and $f(\beta)$ are, respectively, the first and second nonzero terms in the expansion of $\mathcal{I}$ with respect R_0, that read $g(\beta) = (R_0^3/3)[\beta - \sin(2\beta)/2]$ and $f(\beta) = (R_0^4/6)\sin^3(\beta)$. Equations (4), due to the $k > 2$ order fields, require a closure ansatz. This can be done by providing an ansatz on the local order as explained below.

For $\beta \sim \pi$, i.e., (quasi)isotropic interactions, $f \simeq 0$, and we assume that no local order is possible. Under these conditions, Eqs. (4) reduce to

$$\partial_t \rho = -\frac{v_0}{D_\theta}\nabla\left[-\frac{v_0}{2}\nabla\rho + \Gamma g(\beta)\rho\nabla\rho + O(R_0^5)\right], \quad (5)$$

where $O(R_0^5)$ contains spatial third order derivatives with respect to ρ. From Eq. (5), we learn that a homogenous spatial distribution of particles—assume $\rho = \rho_0 + \epsilon\delta\rho$, with ρ_0 a constant and $\epsilon\delta\rho$ a small perturbation—becomes linearly unstable when $c_1 = v_0\Gamma g(\beta)\rho_0/(2D_\theta) - D_{\mathrm{NAP}} > 0$ and the system undergoes phase separation, in absence of orientational order, that leads to the emergence of aggregates as shown in Fig. 1, panels (b) and (c). For $\beta = \pi$, the dispersion relation is of the form $\lambda = c_1\mathbf{k}^2 - c_2\mathbf{k}^4$, where $c_2 = v_0\Gamma\pi R_0^5\rho_0/80 > 0$ and $\mathbf{k}$, the wave number, associates to the perturbation.

For intermediate values of β and D_θ, agent-based simulations display nematic patterns. Let us, then, assume that, locally, the distribution of θ is given by $p(\mathbf{x},\theta,t) \simeq (\rho/2\pi)\exp[(2/\rho)\mathbf{Q}\cdot\mathbf{V}(2\theta)]$ (see [45] for a derivation). As a direct consequence of this local ansatz, we find that $\mathbf{P} = \mathbf{M}_3 = \mathbf{0}$, $M_{4c} = (Q_c^2 - Q_s^2)/(2\rho)$ and $M_{4c} = Q_c Q_s/\rho$. Since, under this assumption, $\mathbf{M}_4$ can be expressed in terms of ρ and $\mathbf{Q}$, Eqs. (4) define a closed set of equations. Now, we look for the stationary states of the resulting system. This implies that all partial temporal derivatives of the fields vanish. For simplicity, but without loss of generality, let us assume that $Q_s = 0$ and that the system is invariant in the $\hat{x}$ direction as in Fig. 4(c), and thus, derivatives in x vanish. Inserting all this into Eqs. (4), we arrive at

$$\partial_y(\rho - Q_c) = -\frac{\Gamma g(\beta)}{v_0}\partial_y\rho(\rho + Q_c) \quad (6a)$$

$$Q_c = -\frac{\Gamma f(\beta)}{8D_\theta}\partial_{yy}\rho\left(\rho - \frac{Q_c^2}{2\rho}\right), \quad (6b)$$

where Q_c and ρ are functions of y. By linearizing this system of equations—assume $\rho = \rho_0 + \epsilon\delta\rho$ and $Q_c = \epsilon\delta Q_c$, with ρ_0 a constant and $\epsilon\delta\rho$ and $\epsilon\delta Q_c$ perturbations in the density and nematic order, respectively, and keeping linear order terms in ϵ—it becomes evident that $\delta Q_c \propto \partial_{yy}\delta\rho$, and the system reduces to $(a\rho_0 - 1)/(b\rho_0)z = \partial_{yy}z$, with $z = \partial_y\delta\rho$, $a = \Gamma g/v_0$, and $b = \Gamma f/(8D_\theta)$, whose solutions for $\rho_0 - 1 < 0$ correspond to trigonometric functions. All this means that, by assuming local nematic order, we can show that: (i) Eqs. (4) exhibit steady state solutions, and (ii) that these static solutions correspond to elongated high density regions, nematically ordered, with $Q_c \propto \rho$, parallel to each other and equally spaced, i.e., there is a well-defined wave length. These solutions are consistent with the nematic bands in Fig. 4.

Finally, we have observed, in agent-based simulations, locally polar patterns (worms). Let us assume, then, that $p(\mathbf{x},\theta,t) \simeq (\rho/2\pi)\exp[(2/\rho)\mathbf{P}\cdot\mathbf{V}(\theta)]$ [45]. Under this assumption, it is possible to show that static polar bands—i.e., static straight worms—cannot exist. The field equations suggest that polar structures never reach a steady state as observed in simulations, see Figs. 1(a) and 3(c).

Concluding remarks.—The derived field equations, combined with the presented numerical study, show that fundamental differences exist between velocity alignment-based models, including polar fluids [12,13,33,53], active nematics [14,35,36], and self-propelled rods [37–40, 42–44,54] on the one hand, and position-based models, such as the one analyzed here, on the other hand. An evident and fundamental difference, revealed by Eqs. (4) and confirmed in simulations, is that position-based models cannot develop either polar or nematic ordered phases that are spatially homogeneous—cf. with the well reported spatially homogeneous ordered phases in (velocity-alignment) flocking models, such as the celebrated Toner-Tu polar phase [12,13,33,53] and homogeneous nematic phase [14,38–40,54]. In contrast, in position-based active models, (orientational) order emerges always, even at short scales, associated to density instabilities. In addition, worms display local polar order that is parallel (locally) to the band, with a highly dynamical center band line that prevents polar long-range order to emerge, in striking difference with polar bands in Vicsek models, where polar order is orthogonal to the band and long ranged [33,53,55]. On the other hand, it has been argued that nematic bands, reported in self-propelled rods [40], are unstable [54]. Again, this is in sharp contrast to the nematic bands reported here that remain stable in the thermodynamical limit. In summary, position-based active systems, such as the one presented here, belong to a new universally active class fundamentally different to any previously reported active matter class [11–14,33–44,53].

Our results could be relevant for studying and interpreting collective patterns in animal groups. They indicate that several flocking patterns observed in nature, such as the millinglike patterns found in fish [4], the file formation reported in sheep herds [6], and the emergence of nematic bands in human crowds and ants [18], could result from simple navigation strategies that do not require memory, use exclusively the instantaneous position of neighboring particles, and limit the interaction neighborhood by a vision cone. These concepts, that lead to navigation strategies that are computationally less intensive than those based on velocity alignment, could help in the design of new robotic navigation algorithms, for instance, as for phototactic robots [56]. Extensions of this minimal cognitive model could find applications in other active systems such as chemophoretic particles [23,28] and chemotactic colloids [57–60] and organisms [61–63], among other examples where aggregation patterns have been reported. This could require either taking $R_0 \to \infty$ or replacing the interaction cutoff by a slowly decaying function of the distance, as well

as specializing the model for $\beta = \pi$, which corresponds to the limit of isotropic interactions, though asymmetric interactions may also be realistic [23,28,61].

We thank C. Beta, C. Condat, M. Polin, R. Soto, and G. Volpe for insightful comments that helped us to reshape the text. L. B. acknowledges financial support from CONICET and F. P. from Agence Nationale de la Recherche via Grant No. ANR-15-CE30-0002-01. Simulations were carried out in CRIMSON and CICADA clusters belonging to OCA and UNSA, respectively.

*peruani@unice.fr

[1] T. Vicsek and A. Zafeiris, Phys. Rep. **517**, 71 (2012).
[2] M. C. Marchetti, J. F. Joanny, S. Ramaswamy, T. B. Liverpool, M. R. J. Prost, and R. A. Simha, Rev. Mod. Phys. **85**, 1143 (2013).
[3] M. Ballerini *et al.*, Proc. Natl. Acad. Sci. U.S.A. **105**, 1232 (2008).
[4] J. Gautrais, F. Ginelli, R. Fournier, S. Blanco, M. Soria, H. Chaté, and G. Theraulaz, PLoS Comput. Biol. **8**, e1002678 (2012).
[5] F. Ginelli, F. Peruani, M.-H. Pillot, H. Chaté, G. Theraulaz, and R. Bon, Proc. Natl. Acad. Sci. U.S.A. **112**, 12729 (2015).
[6] S. Toulet, J. Gautrais, R. Bon, and F. Peruani, PLoS One **10**, e0140188 (2015).
[7] D. Grossman, I. Aranson, and E. Ben-Jacob, New J. Phys. **10**, 023036 (2008).
[8] J. Deseigne, O. Dauchot, and H. Chaté, Phys. Rev. Lett. **105**, 098001 (2010).
[9] C. A. Weber, T. Hanke, J. Deseigne, S. Léonard, O. Dautchot, E. Frey, and H. Chaté, Phys. Rev. Lett. **110**, 208001 (2013).
[10] K.-D. N. T. Lam, M. Schindler, and O. Dauchot, New J. Phys. **17**, 113056 (2015).
[11] T. Vicsek, A. Czirok, E. Ben-Jacob, I. Cohen, and O. Shochet, Phys. Rev. Lett. **75**, 1226 (1995).
[12] J. Toner and Y. Tu, Phys. Rev. Lett. **75**, 4326 (1995).
[13] J. Toner and Y. Tu, Phys. Rev. E **58**, 4828 (1998).
[14] S. Ramaswamy, R. A. Simha, and J. Toner, Europhys. Lett. **62**, 196 (2003).
[15] S. Ramaswamy, Annu. Rev. Condens. Matter Phys. **1**, 323 (2010).
[16] P. Romanczuk, I. D. Couzin, and L. Schimansky-Geier, Phys. Rev. Lett. **102**, 010602 (2009).
[17] D. Strömbom, J. Theor. Biol. **283**, 145 (2011).
[18] M. Moussaid, D. Helbing, and G. Theraulaz, Proc. Natl. Acad. Sci. U.S.A. **108**, 6884 (2011).
[19] D. J. G. Pearce, A. M. Miller, G. Rowlands, and M. S. Turner, Proc. Natl. Acad. Sci. U.S.A. **111**, 10422 (2014).
[20] E. Ferrante, A. E. Turgut, M. Dorigo, and C. Huepe, Phys. Rev. Lett. **111**, 268302 (2013).
[21] C. Huepe, E. Ferrante, T. Wenseleers, and A. Turgut, J. Stat. Phys. **158**, 549 (2015).
[22] R. Grossmann, L. Schimansky-Geier, and P. Romanczuk, New J. Phys. **15**, 085014 (2013).
[23] R. Soto and R. Golestanian, Phys. Rev. Lett. **112**, 068301 (2014).
[24] J. J. Gibson, The British Journal of clinical psychology **49**, 182 (1958).
[25] D. M. McComb and S. M. Kajiura, J. Exp. Biol. **211**, 482 (2008).
[26] A. Strandburg-Peshkin *et al.*, Curr. Biol. **23**, R709 (2013).
[27] J. Dzubiella, H. Löwen, and C. N. Likos, Phys. Rev. Lett. **91**, 248301 (2003).
[28] A. V. Ivlev, J. Bartnick, M. Heinen, C.-R. Du, V. Nosenko, and H. Löwen, Phys. Rev. X **5**, 011035 (2015).
[29] L. P. Dadhichi, R. Chajwa, A. Maitra, and S. Ramaswamy, arXiv:1605.00981.
[30] A. Cavagna, I. Giardina, A. Jelic, E. Silvestri, and M. Viale, arXiv:1605.00986.
[31] P. T. Nguyen, S.-H. Lee, and V. T. Ngo, Phys. Rev. E **92**, 032716 (2015).
[32] M. Durve and A. Sayeed, Phys. Rev. E **93**, 052115 (2016).
[33] H. Chaté, F. Ginelli, G. Grégoire, and F. Raynaud, Phys. Rev. E **77**, 046113 (2008).
[34] J. Toner, Phys. Rev. E **86**, 031918 (2012).
[35] H. Chaté, F. Ginelli, and R. Montagne, Phys. Rev. Lett. **96**, 180602 (2006).
[36] S. Ngo, A. Peshkov, I. S. Aranson, E. Bertin, F. Ginelli, and H. Chaté, Phys. Rev. Lett. **113**, 038302 (2014).
[37] F. Peruani, A. Deutsch, and M. Bär, Phys. Rev. E **74**, 030904(R) (2006).
[38] F. Peruani, A. Deutsch, and M. Bär, Eur. Phys. J. Spec. Top. **157**, 111 (2008).
[39] A. Baskaran and M. C. Marchetti, Phys. Rev. Lett. **101**, 268101 (2008).
[40] F. Ginelli, F. Peruani, M. Bär, and H. Chaté, Phys. Rev. Lett. **104**, 184502 (2010).
[41] A. Peshkov, I. S. Aranson, E. Bertin, H. Chaté, and F. Ginelli, Phys. Rev. Lett. **109**, 268701 (2012).
[42] M. Abkenar, K. Marx, T. Auth, and G. Gompper, Phys. Rev. E **88**, 062314 (2013).
[43] S. Weitz, A. Deutsch, and F. Peruani, Phys. Rev. E **92**, 012322 (2015).
[44] D. Nishiguchi, K. H. Nagai, H. Chaté, and M. Sano, arXiv:1604.04247.
[45] See Supplemental Material at http://link.aps.org/supplemental/10.1103/PhysRevLett.117.248001, for further technical details and movies, which includes Refs. [46,47].
[46] M. Doi and S. F. Edwards, *The Theory of Polymer Dynamics* (Oxford University Press, New York, 1986).
[47] H. Risken, *The Fokker-Planck Equation* (Springer, New York, 1988).
[48] From [4,5,25], we expect $\beta \in [0.5, \pi]$ (radians), $0.005\ \mathrm{s}^{-1} \leq \sqrt{2D_\theta} \leq 2\ \mathrm{s}^{-1}$, $v_0 \sim 1$ m/s, $1\ \mathrm{s}^{-1} < \gamma < 10\ \mathrm{s}^{-1}$, and $R_0 \in [1\mathrm{m}, 20\mathrm{m}]$.
[49] M. R. D'Orsogna, Y. L. Chuang, A. L. Bertozzi, and L. S. Chayes, Phys. Rev. Lett. **96**, 104302 (2006).
[50] J. Tailleur and M. E. Cates, Phys. Rev. Lett. **100**, 218103 (2008).
[51] F. D. C. Farrell, M. C. Marchetti, D. Marenduzzo, and J. Tailleur, Phys. Rev. Lett. **108**, 248101 (2012).
[52] E. Mones, E. A. Czirok, and T. Vicsek, New J. Phys. **17**, 063013 (2015).

[53] E. Bertin, M. Droz, and G. Grégoire, J. Phys. A **42**, 445001 (2009).
[54] A. Peshkov, I. S. Aranson, E. Bertin, H. Chate, and F. Ginelli, Phys. Rev. Lett. **109**, 268701 (2012).
[55] G. Grégoire and H. Chaté, Phys. Rev. Lett. **92**, 025702 (2004).
[56] M. Mijalkov, A. McDaniel, J. Wehr, and G. Volpe, Phys. Rev. X **6**, 011008 (2016).
[57] O. Pohl and H. Stark, Phys. Rev. Lett. **112**, 238303 (2014).
[58] S. Saha, R. Golestanian, and S. Ramaswamy, Phys. Rev. E **89**, 062316 (2014).
[59] B. Liebchen, D. Marenduzzo, I. Pagonabarraga, and M. E. Cates, Phys. Rev. Lett. **115**, 258301 (2015).
[60] A. Zöttl and H. Stark, J. Phys. Condens. Matter **28**, 253001 (2016).
[61] L. L. Soon, IUBMB Life **59**, 60 (2007).
[62] G. Amselem, M. Theves, A. Bae, E. Bodenschatz, and C. Beta, PLoS One **7**, e37213 (2012).
[63] C. Westendorf, J. Negrete, A. Bae, R. Sandmanna, E. Bodenschatz, and C. Beta, Proc. Natl. Acad. Sci. U.S.A. **110**, 3853 (2013).